Ergodic Capacity of Hard-Switching in Hybrid FSO/IRS-Assisted RF Transmission

Soumen Mondal[†], Dipen Bepari[*] Keshav Singh[†], and Aryan Kaushik[‡]
[†]Institute of Communications Engineering, National Sun Yat-sen University, Kaohsiung 80424, Taiwan
[*]Department of Electronics and Communication Engineering, Indian Institute of Information Technology, Pune, India
[‡]Department of Computing and Mathematics, Manchester Metropolitan University, UK
E-mail: soumen.durgapur@gmail.com, dipen@iiitp.ac.in, keshav.singh@mail.nsysu.edu.tw, a.kaushik@mmu.ac.uk

***Abstract*—This paper presents an ergodic capacity analysis of a hybrid free-space optical (FSO)/Radio-Frequency (RF) communication system with hard-switching scheme. The RF transmission is assisted by an intelligent reflecting surface (IRS). The larger bandwidth FSO link is considered as the primary communication link and the RF link having lower bandwidth is considered as the secondary communication link. When the signal-to-noise ratio (SNR) of the FSO link drops below an acceptable level, the communication link switches from the primary FSO link to the secondary RF link, and the RF transmission is assisted by an IRS. The ergodic capacity of the mixed IRS-aided RF/FSO system is derived and validated via Monte Carlo simulations. The influence of IRS element count on ergodic capacity has been elucidated, particularly at the lower SNR of the FSO link for both moderate and strong turbulences. The variation of ergodic capacity with source-destination link distance is also presented.**

***Index Terms*—Free-space optical, Hard-switching, Meijer G-function, Capacity.**

I. Introduction

FREE-space optical (FSO) communication is a fast emerging and cost-effective communication technology that can be easily deployed [1]. It uses an unregulated frequency band near-infrared radiation (IR) band. In addition, it is immune to interference and noise due to the non-broadcasting characteristic of the optical beam. Despite these compelling features of FSO communication, data transmission through FSO link suffers from signal degradation due to turbulence in the atmosphere along with adverse weather conditions such as fog and haze. The Gamma-Gamma (GG) distribution is widely used to characterize the optical channel under moderate and strong turbulence conditions [2]. Further, misalignment between transmitter and receiver due to building sway and weak earthquake gives rise to an impairment in FSO communication referred to as pointing error [3]. On the other hand, the communication through the lower bandwidth RF link is robust to atmospheric turbulence. These complementary characteristics of FSO and RF can be exploited in hybrid RF/FSO communication system to better extract desirable features of both the links.

Several schemes to combine RF and FSO links such as series combination [4], parallel combination [5], adaptive combining [6], and hard-switching [7] have been discussed in the recent research articles. The combination of RF and FSO links in the series may suffer if either of the two links is poor [4]. This limitation can be mitigated by having both the FSO and the RF links connected in parallel and by simultaneously deploying both links [5]. Further, several diversity scheme like selection combining (SC) [8], maximal ratio combining (MRC) [5] schemes are utilized to improve performance at the cost of multiple antennas. The adverse effects of a lower bandwidth RF link is diluted if the link quality of the larger bandwidth FSO link is good. However, this can be considered as under-utilization of the RF link. Recently, an adaptive diversity scheme has been adopted in a hybrid RF/FSO communication where the FSO link is always available for transmission [6]. The RF backup link is triggered only if the FSO link fails to meet the required threshold quality. The basic disadvantage of this scheme is that the FSO link continues to operate and draw power, even under poor channel conditions. The aforementioned issues are resolved in hard-switching where only one of the links is allowed to transmit a signal at any point in time depending on the signal-to-noise ratio (SNR). To be specific, under low complexity hard-switching, the data transmission is carried out through a primary FSO link as long as its SNR is above a specific threshold and the RF link is activated if its SNR falls below that threshold [7]. An RF backup link is used for communication in a two-hop network [9], however, this system model is limited to a single antenna or single aperture setup. Recently, hard switching has been implemented between FSO and THz for terrestrial communication [10].

However, blockages severely affect communication through any RF link. The loss in performance due to blockages can be compensated by utilizing alternate propagation links via metamaterial-based passive surfaces known as intelligent reconfigurable surfaces (IRS) [11]. Each element of IRS is programmed in such a way that all the reflecting waves combine coherently at the destination yielding passive beamforming gains and boost in the receive signal strength [12][1]. The performance of a hybrid relay and IRS-assisted wireless network has been studied in [14]. The IRS was introduced to assist RF transmission in hybrid FSO/RF system first in [15], the links are placed in series. The

This work was supported in part by the National Science and Technology Council of Taiwan under Grant 113-2218-E-110-009 and also in part by the Sixth Generation Communication and Sensing Research Center funded by the Higher Education SPROUT Project, Ministry of Education of Taiwan.

[1]The phases at each element of IRS can be programmed from the source using an FPGA based controller and a dedicated control link [12], [13].

979-8-3315-6946-4/25/$31.00 ©2025 IEEE

similar system model as in [15] is extended with multiple transmit optical apertures for minimizing turbulence effects and outage and the bit error rate has been evaluated with co-channel interference [16]. In [17], the authors studied a hybrid backhaul-fronthaul system for NOMA network, where backhaul communication uses an FSO link, and fronthaul relies on an RF link assisted by an active IRS. However, the work is limited to a single-input single-output scenario. Furthermore, this network has been extended to a multiple-input single-output setup in [18].

The above-mentioned work related to hybrid FSO and IRS-aided RF communication [15], [16] has considered that FSO and RF link are in series arrangement. Hence, disruption in any link may disrupt the end-to-end connectivity. Specifically, disruption of RF links due to blockage may waste the high-speed FSO link resource. The severity of blockage of RF signal can be mitigated with IRS technology. This motivates us to analyze the ergodic capacity of hybrid FSO and IRS-assisted RF transmission under hard-switching. To the authors' knowledge, noprior studies have yet analyzed the ergodic capacity of a hybrid FSO and IRS-assisted RF system based on a hard-switching scheme. To this end, in this work, a novel closed-form expression for ergodic capacity has been derived for the FSO/IRS-aided RF communication system under hard-switching scheme and expressed in terms of MeijerG function. The primary contributions of this paper are outlined below:

- An analytical expression in closed-form for ergodic capacity has been derived for hard-switching based hybrid FSO/RF system considering Gamma-Gamma and Rayleigh distributions for characterizing FSO and RF links, respectively.
- The impact of the number of phase-shifter elements at IRS on ergodic capacity has been presented.
- The role of atmospheric turbulence and the source-destination link distance on the ergodic capacity have been presented.

The rest of the paper is structured as follows: Section II introduces the system model, including optical and RF channel modeling. The ergodic capacity analysis is presented in Section III. The findings and associated discussions are outlined in Section IV. Section V provides the conclusions of the paper.

II. System and Channel Modeling

A hybrid IRS-aided RF/FSO communication-based network, in which an IRS with N passive elements assists RF transmission under hard-switching is considered as depicted in Fig. 1. The source (s) and destination (d) each feature a single RF antenna and a single optical aperture.

Under the hard-switching system model, the larger bandwidth primary FSO link switches to a back-up RF link, when the optical received signal strength drops below a threshold. On the contrary, when the optical received signal strength is above an acceptable level, the primary FSO link is restored and RF link is idle. In practice, it is the receiver that monitors the SNR and conveys the information to the transmitter via

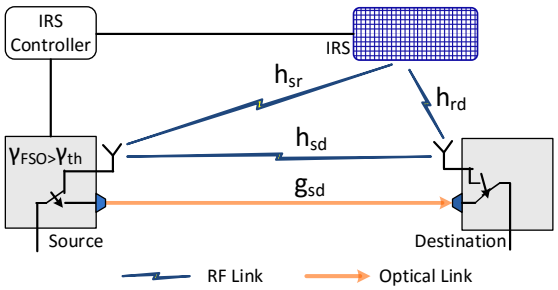

Fig. 1: System Model.

a feedback loop in case the SNR goes above/below the threshold so that the transmitter may switch to the FSO/RF link.

Under hard-switching configuration, signal is transmitted through FSO link, if the link quality of the optical channel is above an acceptable level and RF link is idle. On the contrary, when FSO link quality drops below the acceptable level, the secondary RF channel is activated. Thus, under hard-switching configuration, the destination receives either optical signal or RF signal at any point in time.

Optical Channel Modeling: The intensity of the optical signal fluctuates due to atmospheric fading-induced turbulence. The reason behind the fluctuation in the optical signal intensity is the variation of refractive index due to variations in temperature, humidity, etc. The received SNR at the destination through an optical link can be expressed as $\gamma_{\rm op} = \bar{\gamma}_{\rm op}|g_{\rm sd}|^2$, where $\bar{\gamma}_{\rm op} = \frac{\eta P_{\rm op}}{\sigma^2_{\rm op}}$. The optical-to-electrical transformation coefficient is η $(0 \leq \eta \leq 1)$, $P_{\rm op}$ and $\sigma^2_{\rm op}$ denote the transmit power and noise variance of optical link, respectively.

Considering ideal alignment between the optical transmitter and receiver, the probability density function (PDF) of $\gamma_{\rm op}$ modeled by GG distribution can be written as [2]

$$f_{\gamma_{\rm op}}(z) = \frac{1}{2z\Gamma(\alpha)\Gamma(\beta)} G^{2,0}_{0,2}\left(\alpha\beta\sqrt{\frac{z}{\bar{\gamma}_{\rm op}}}\,\middle|\, \begin{matrix} - \\ \alpha, \beta \end{matrix}\right), \quad (1)$$

where, $\Gamma(\cdot)$ denotes complete Gamma function and $G^{-,-}_{-,-}\left(z|^{::}_{::}\right)$ denotes Meijer G-function [19]. The scintillation parameters α and β are given by [1].

$$\alpha = \left[\exp\left(\frac{0.49\sigma_{\rm r}^2}{\left(1+1.11\sigma_{\rm r}^{12/5}\right)^{7/6}}\right) - 1\right]^{-1}, \quad (2)$$

$$\beta = \left[\exp\left(\frac{0.51\sigma_{\rm r}^2}{\left(1+0.69\sigma_{\rm r}^{12/5}\right)^{5/6}}\right) - 1\right]^{-1}. \quad (3)$$

Furthermore, $\sigma_{\rm r}^2 = 1.23 C_{\rm n}^2 k^{7/6} d_{\rm sd}^{11/6}$ denotes the Rytov variance, $k = 2\pi/\lambda_{\rm op}$ denotes the optical wave number, $C_{\rm n}^2$ captures the strength of the turbulence and $L_{\rm sd}$ represents the distance between source and destination. The corresponding cumulative distribution function (CDF) can be derived using

the identity in [20, Eq. 07.34.21.0084.01] as

$$F_{\gamma_{\rm op}}(z) = \frac{2^{\alpha+\beta-2}}{\pi\Gamma(\alpha)\Gamma(\beta)} G_{1,5}^{4,1}\left(\frac{\alpha^2\beta^2 z}{16\overline{\gamma}_{\rm op}}\middle| \begin{matrix} 1 \\ \chi_1 \end{matrix}\right), \quad (4)$$

where, $\chi_1 = \left\{\frac{\alpha}{2}, \frac{\alpha+1}{2}, \frac{\beta}{2}, \frac{\beta+1}{2}, 0\right\}$. The CDF of $\gamma_{\rm op}$ can be derived in an alternate form from Eq. (1) using [20, Eq. 07.34.21.0085.01] and expressed as

$$\begin{aligned} F_{\gamma_{\rm op}}(z) &= 1 - \int_z^{\infty} f_{\gamma_{\rm op}}(t)dt, \\ &= 1 - \frac{2^{\alpha+\beta-2}}{\pi\Gamma(\alpha)\Gamma(\beta)} G_{1,5}^{5,0}\left(\frac{\alpha^2\beta^2 z}{16\overline{\gamma}_{\rm op}}\middle| \begin{matrix} 1 \\ \chi_1 \end{matrix}\right). \end{aligned} \quad (5)$$

RF Channel modeling: The signal received through RF link considering both the source-destination direct channel ($h_{\rm sd}$) and the channels via the IRS is given by

$$y_{\rm rf} = \sqrt{P_{\rm rf}}\left(h_{\rm sd} + \mathbf{h}_{\rm sr}^T \mathbf{\Phi} \mathbf{h}_{\rm rd}\right) x + w_{\rm rf}, \quad (6)$$

where $P_{\rm rf}$ is the RF transmit power. The IRS-destination channel vector $\mathbf{h}_{\rm rd} = [h_{{\rm rd},1}, \ldots, h_{{\rm rd},N}]^T \in \mathbb{C}^{N{\rm x}1}$, and the receiver noise $w_{\rm rf} \sim \mathcal{CN}(0, \sigma_{\rm rf}^2)$ where $\sigma_{\rm rf}^2 = N_0 B_{\rm rf} + N_{\rm F}$ is the variance of the AWGN and N_0 denotes the noise power spectral density, $N_{\rm F}$ is the noise figure of the RF link and $B_{\rm rf}$ is the bandwidth of the RF link. Furthermore, the source-IRS channel vector $\mathbf{h}_{\rm sr}^T = [h_{{\rm sr},1}, \ldots, h_{{\rm sr},N}] \in \mathbb{C}^{1{\rm x}N}$. Note that $h_{{\rm rd},n}$ and $h_{{\rm sr},n}$ denote the channel between the $n^{\rm th}$ phase-shifter at the IRS and destination, and the source and the $n^{\rm th}$ phase-shifter at the IRS, respectively. All the individual channels are assumed to be uncorrelated Rayleigh faded. Thus, $h_{\rm sd} \sim \mathcal{CN}(\mathbf{0}, \mu_{\rm sd})$, $\mathbf{h}_{\rm sr} \sim \mathcal{CN}(\mathbf{0}, \mu_{\rm sr}\mathbf{I}_{\rm N})$, and $\mathbf{h}_{\rm rd} \sim \mathcal{CN}(\mathbf{0}, \mu_{\rm rd}\mathbf{I}_{\rm N})$, where $\mu_{\rm sd}$, $\mu_{\rm sr}$, and $\mu_{\rm rd}$ capture the path-loss of the corresponding links. The path-loss has been characterized based on the 3GPP urban micro model (UMi) at 3 GHz [13, Eq. 23].

$$\mu_i = \mathcal{G}_{\rm t} + \mathcal{G}_{\rm r} - 35.1 - 36.7\log_{10}(L_i), \quad (7)$$

where, L_i is the link distance between source and destination, $\mathcal{G}_{\rm t}$ and $\mathcal{G}_{\rm r}$ denote antenna gain at the transmitter and the receiver (dBi), respectively, and $i \in \{{\rm sr}, {\rm rd}, {\rm sd}\}$. The IRS phase-shift matrix $\mathbf{\Phi} = {\rm diag}\left(e^{j\phi_1}, ..., e^{j\phi_{\rm N}}\right) \in \mathbb{C}^{N{\rm x}N}$, where $\phi_n \in [0, 2\pi)$. The received SNR over the RF link is expressed as

$$\gamma_{\rm rf} = \bar{\gamma}_{\rm rf}\left|h_{\rm sd} + \mathbf{h}_{\rm sr}^T \mathbf{\Phi} \mathbf{h}_{\rm rd}\right|^2, \quad (8)$$

where $\bar{\gamma}_{\rm rf} = \frac{P_{\rm rf}}{\sigma_{\rm rf}^2}$. The optimal ϕ_n that maximizes the receive SNR is $\phi_n^* = \arg(h_{\rm sd}) - \arg(h_{{\rm sr},n}) - \arg(h_{{\rm rd},n}) = \phi_{\rm sd} - (\phi_{{\rm sr},n} + \phi_{{\rm rd},n})$ [13].

$$\begin{aligned} \phi_n^* &= \arg(h_{\rm sd}) - \arg(h_{{\rm sr},n}) - \arg(h_{{\rm rd},n}) \\ &= \phi_{\rm sd} - (\phi_{{\rm sr},n} + \phi_{{\rm rd},n}). \end{aligned} \quad (9)$$

The SNR of RF link assuming optimal phase shift can be expressed as [13]

$$\begin{aligned} \gamma_{\rm rf} &= \max_{\phi_1,\ldots,\phi_N} \bar{\gamma}_{\rm rf}\left|h_{\rm sd} + \mathbf{h}_{\rm sr}^T \mathbf{\Phi} \mathbf{h}_{\rm rd}\right|^2, \\ &= \bar{\gamma}_{\rm rf}\left||h_{\rm sd}| + \sum\nolimits_{n=1}^{N} |h_{{\rm sr},n}|\,|h_{{\rm rd},n}|\right|^2, \end{aligned} \quad (10)$$

The CDF of SNR of the RF link is expressed as [21],

$$F_{\gamma_{\rm rf}}(z) = 1 - \frac{\Gamma\left(\delta_0, \frac{\sqrt{z}}{\Omega_0}\right)}{\Gamma(\delta_0)}, \quad (11)$$

where $\Gamma(\cdot,\cdot)$ denotes upper incomplete Gamma function, $\delta_0 = \frac{(\sqrt{\mu_{\rm sd}\pi} + 2N\delta w)^2}{4\mu_{\rm sd} + 4N\delta w^2 - \mu_{\rm sd}\pi}$, $\Omega_0 = \sqrt{\bar{\gamma}_{\rm rf}}\left(\frac{4\mu_{\rm sd} + 4N\delta\Omega^2 - \mu_{\rm sd}\pi}{2(\sqrt{\mu_{\rm sd}\pi} + 2N\delta\Omega)}\right)$, $\delta = \pi^2/(16 - \pi^2)$, and $\Omega = (4 - \pi^2/4)\sqrt{\mu_{\rm sr}\mu_{\rm rd}}/\pi$.
The PDF of $\gamma_{\rm rf}$ is given by [22],

$$f_{\gamma_{\rm rf}}(z) = \frac{z^{\frac{\delta_0-2}{2}} e^{-\frac{\sqrt{z}}{\Omega_0}}}{2\Gamma(\delta_0)\Omega_0{}^{\delta_0}}. \quad (12)$$

III. Ergodic Capacity Analysis

In hard-switching scheme, the transmission link switches from FSO to RF link when $\gamma_{\rm op}$ falls below the threshold level ($\gamma_{\rm th}^{\rm op}$) and the SNR at the destination is represented by

$$\gamma_{\rm e2e} = \begin{cases} \gamma_{\rm op}, & \gamma_{\rm op} \geq \gamma_{\rm th}^{\rm op}, \quad \text{Case-I: FSO Link,} \\ \gamma_{\rm rf}, & \gamma_{\rm op} < \gamma_{\rm th}^{\rm op}, \quad \text{Case-II: RF Link.} \end{cases} \quad (13)$$

Based on Eq. (13), the ergodic capacity is given by

$$\begin{aligned} \bar{C}_{\rm Total} &= \bar{C}_{\rm op} + P_r\{\gamma_{\rm op} < \gamma_{\rm th}^{\rm op}\}\bar{C}_{\rm rf}, \\ &= \bar{C}_{\rm op} + F_{\gamma_{\rm op}}(\gamma_{\rm th}^{\rm op})\bar{C}_{\rm rf}, \end{aligned} \quad (14)$$

where $\bar{C}_{\rm op}$ represents the capacity when the FSO link is active ($\gamma_{\rm op} \geq \gamma_{\rm th}^{\rm op}$) and $\bar{C}_{\rm rf}$ represents the capacity when the RF link is active ($\gamma_{\rm op} < \gamma_{\rm th}^{\rm op}$). The ergodic capacity when the FSO link is active equals

$$\begin{aligned} \overline{C}_{\rm op} &= \int_{\gamma_{\rm th}^{\rm op}}^{\infty} \log_2(1+z) f_{\gamma_{\rm op}}(z) dz, \\ &\overset{(a)}{=} \frac{1}{\ln(2)} \underbrace{\int_{\gamma_{\rm th}^{\rm op}}^{\infty} \frac{1 - F_{\gamma_{\rm op}}(z)}{1+z} dz}_{I_1} + \frac{1}{\ln(2)} \underbrace{\ln(1+\gamma_{\rm th}^{\rm op})\left(1 - F_{\gamma_{\rm op}}(\gamma_{\rm th}^{\rm op})\right)}_{I_2}. \end{aligned} \quad (15)$$

To simply Eq. (15), the integration by parts and some algebraic rearrangement are applied in step (a).
The term I_1 can be derived using the expression $F_{\gamma_{\rm op}}(z)$ given in Eq. (4). The identities in [20, Eq. 07.34.03.0271.01] and [23, Eq. 2.24.1.3] are applied in step (b) and step (c), respectively, and through a change of limit in step (b), use of identity $\frac{1}{x+A} = \frac{1}{A} G_{1,1}^{1,1}\left(\frac{x}{A}\middle| \begin{matrix} 0 \\ 0 \end{matrix}\right)$ [20, Eq. 07.34.03.0271.01], change of variable, and through the application of identity [23, Eq. 2.24.1.3] in step (c).

$$\begin{aligned} I_1 &= \int_{\gamma_{\rm th}^{\rm op}}^{\infty} \frac{1 - F_Z(z)}{1+z} dz, \\ &\overset{(b)}{=} \frac{2^{\alpha+\beta-2}}{\pi\Gamma(\alpha)\Gamma(\beta)} \int_0^{\infty} \frac{1}{\gamma_{\rm th}^{\rm op}+1} G_{1,1}^{1,1}\left(\frac{t}{\gamma_{\rm th}^{\rm op}+1}\middle| \begin{matrix} 0 \\ 0 \end{matrix}\right) \\ &\qquad \times G_{1,5}^{5,0}\left(Bt + \gamma_{\rm th}^{\rm op} B\middle| \begin{matrix} 1 \\ \chi_1 \end{matrix}\right) dt, \\ &\overset{(c)}{=} \frac{2^{\alpha+\beta-2}}{\pi\Gamma(\alpha)\Gamma(\beta)B(\gamma_{\rm th}^{\rm op}+1)} \sum_{k=0}^{\infty} \frac{(-\gamma_{\rm th}^{\rm op} B)^k}{k!} G_{7,3}^{1,7}\left(\frac{1}{B(\gamma_{\rm th}^{\rm op}+1)}\middle| \begin{matrix} \chi_2 \\ \chi_3 \end{matrix}\right). \end{aligned} \quad (16)$$

Table I: Values of I_1 for different summation limits.

K	$P_{\rm op} = 30\,$dBm	$P_{op} = 40\,$dBm	K_{rq}
49	3.2702463793997	**5.5728077**604400	51
51	**3.2702447**637846	**5.5728077**374576	
53	**3.2702443**161798	**5.5728077**169719	
57	3.2702440138382	**5.5728076**986327	

where, $\chi_2 = \left\{0, 0, k, k-\frac{\alpha}{2}, k-\frac{\alpha+1}{2}, k-\frac{\beta}{2}, k-\frac{\beta+1}{2}\right\}$, $\chi_3 = \{0, k-1, k\}$, and $B = \frac{\alpha^2\beta^2}{16\bar{\gamma}_{\rm op}}$.
Meanwhile, I_2 can be expressed as

$$\begin{aligned} I_2 &= \ln(1+\gamma_{\rm th}^{\rm op})\,(1 - F_X(\gamma_{\rm th}^{\rm op})), \\ &= \ln(1+\gamma_{\rm th}^{\rm op}) \frac{2^{\alpha+\beta-2}}{\pi\Gamma(\alpha)\Gamma(\beta)} G_{1,5}^{5,0}\left(\gamma_{\rm th}^{\rm op} B \,\middle|\, \begin{matrix} 1 \\ \chi_1 \end{matrix}\right), \end{aligned} \quad (17)$$

where, $\chi_1 = \left\{\frac{\alpha}{2}, \frac{\alpha+1}{2}, \frac{\beta}{2}, \frac{\beta+1}{2}, 0\right\}$.
Using the expression of $F_{\gamma_{\rm rf}}(z)$ in Eq.(11), [20, Eq. 07.34.03.0613.01, Eq. 07.34.21.0086.01], the analytical expression for the ergodic capacity of the RF link can be derived as

$$\begin{aligned} \overline{C}_{\rm rf} &= \frac{1}{\ln(2)} \int_0^\infty \frac{\Gamma\left(\delta_0, \frac{\sqrt{z}}{\Omega_0}\right)}{\Gamma(\delta_0)\,(1+z)} dz, \\ &= \frac{1}{\ln(2)\Gamma(\delta_0)} \int_0^\infty \frac{1}{(1+z)} G_{1,2}^{2,0}\left(\frac{\sqrt{z}}{\Omega_0} \,\middle|\, \begin{matrix} 1 \\ \delta_0, 0 \end{matrix}\right) dz, \\ &= \frac{2^{\delta_0-1}(\pi)^{-\frac{1}{2}}}{\ln(2)\Gamma(\delta_0)} G_{3,5}^{5,1}\left(\frac{1}{4\Omega_0^2} \,\middle|\, \begin{matrix} 0, \frac{1}{2}, 1 \\ 0, \frac{\delta_0}{2}, \frac{\delta_0+1}{2}, 0, \frac{1}{2} \end{matrix}\right). \end{aligned} \quad (18)$$

Substituting Eqs. (4), (16), (17), and (18) into (14), closed-form expression of ergodic capacity is obtained and given in Eq. (19) at the top of next page.

The Cauchy ratio test (CRT) has been applied for convergence test of the infinite series of I_1 in Eq. (16). As per CRT, the infinite series is convergent if $\lim_{k\to\infty} \left|\frac{T_{k+1}}{T_k}\right| < 1$. Here, $T_k = \frac{\left(-\gamma_{\rm th}^{\rm op} B\right)^k}{k!} G_{7,3}^{1,7}\left(\frac{1}{B\left(\gamma_{\rm th}^{\rm op}+1\right)} \,\middle|\, \begin{matrix} \chi_2^{(k)} \\ \chi_3^{(k)} \end{matrix}\right)$ is the $k^{\rm th}$ term of I_1, $\chi_2^{(k)} = \left\{0, 0, k, k-\frac{\alpha}{2}, k-\frac{\alpha+1}{2}, k-\frac{\beta}{2}, k-\frac{\beta+1}{2}\right\}$, and $\chi_3^{(k)} = \{0, k-1, k\}$. Therefore,

$$\left|\frac{T_{k+1}}{T_k}\right| = \left|\frac{-\gamma_{\rm th}^{\rm op} B}{k+1}\Gamma\right| = \left|-\frac{\gamma_{\rm th}^{\rm op}\alpha^2\beta^2}{16\bar{\gamma}_{\rm op}(k+1)}\Gamma\right|, \quad (20)$$

where
$\Gamma = G_{7,3}^{1,7}\left(\frac{1}{B\left(\gamma_{\rm th}^{\rm op}+1\right)} \,\middle|\, \begin{matrix} \chi_2^{(k+1)} \\ \chi_3^{(k+1)} \end{matrix}\right) / G_{7,3}^{1,7}\left(\frac{1}{B\left(\gamma_{\rm th}^{\rm op}+1\right)} \,\middle|\, \begin{matrix} \chi_2^{(k)} \\ \chi_3^{(k)} \end{matrix}\right)$.
Note that Γ represents the ratio of two Meijer G-function is always a non-zero-real number [24]. As $k \to \infty$, $\left|\frac{\Gamma_{k+1}}{\Gamma_k}\right| \to 0$ because the rate of decrease by $(k+1)$ in Eq. (20) dominates over rate of increase of Γ with k [24].

In order to reduce computation time, the summation of infinite terms in I_1 in Eq. (16) can be truncated into a summation of finite terms $(K_{\rm rq})$ with negligible loss of the order of 10^{-6} as shown in Table I. The effective value of $\bar{C}_{\rm op}$ in Eq. (16) and corresponding $\bar{C}_{\rm Total}$ in Eq. (19) is not affected upto sixth decimal points. The Fig. 2 shows the values of I_1 as a function of number of terms in I_1. It is noticeable from Fig. 2 that values of I_1 remains unaltered upto sixth digit after $K_{\rm rq} = 51$ for $P_{\rm op} = 30\,$dBm and $K_{\rm rq} < 49$ for $P_{\rm op} = 40\,$dBm. The value of the $\gamma_{\rm th}^{\rm op}$ is set at $40\,$dB, the source-destination link distance is considered as $600\,$m under strong turbulence environment. The values of I_1 is tabulated for different values of $K_{\rm rq}$. For generating the analytical results, we have taken $K_{\rm rq} = 80$.

Table II: Optical channel Parameters

Turbulence	Link distance	$C_{\rm n}^2(m^{-2/3})$	α	β
Strong	600 m	1×10^{-13}	4.789	3.070
Moderate	600 m	3×10^{-14}	10.232	8.719
Strong	800 m	1×10^{-13}	4.123	2.135

Table III: System Parameters

Parameter	Symbol	Value
Source-destination link distance	$L_{\rm sd}$	600 m
Source-IRS link distance	$L_{\rm sr}$	560 m
IRS-destination link distance	$L_{\rm rd}$	60 m
Optical wavelength	$\lambda_{\rm op}$	1550 nm
Optical transmit power	$P_{\rm op}$	$0 - 40\,$dBm
Noise variance in optical link	$\sigma_{\rm op}^2$	10^{-7}
Optical-to-electrical transfer coefficient	η	0.5
RF wavelength	$\lambda_{\rm r}$	10 cm
RF carrier frequency	$f_{\rm c}$	3 GHz
RF antenna gain	$\mathcal{G}_{\rm t}$, $\mathcal{G}_{\rm r}$	10 dBi
RF receiver antenna gain	$\mathcal{G}_{\rm r}$	10 dBi
RF transmit power	$P_{\rm rf}$	10, 5 dBm
RF noise figure	N_F	10 dB
Noise power spectral density	N_0	$-114\,$dBm/MHz
Strong turbulence strength	C_n^2	$1{\times}10^{-13}m^{-2/3}$
Moderate turbulence strength	C_n^2	$3{\times}10^{-14}m^{-2/3}$

IV. Results and Discussions

In this section, results are presented to evaluate ergodic capacity under hard-switching configurations with different turbulences and different link distances. The parameters used for the analysis are given in Table II and Table III.

Fig. 3 shows the ergodic capacity of hybrid RF/FSO system as a function of the transmit power of FSO link ($P_{\rm op}$) for different numbers of reflected elements at IRS under strong turbulence. The $d_{\rm sd}$, $d_{\rm sr}$, and d_{rd} are considered as $500\,$m, $460\,$m, and $60\,$m, respectively. The ergodic capacity for the transmission through a single FSO link only is very low for lower values of $P_{\rm op}$ and monotonically increases as $P_{\rm op}$ increases. In hybrid RF/FSO system, the RF link is active for transmission at lower $P_{\rm op}$. All the parameters involved in RF link is kept fixed, thus, the ergodic capacity remains constant for lower values of $P_{\rm op}$. It is observed that the ergodic capacity increases marginally as the number of IRS elements increases in this regime. With increase of the FSO transmit power, RF link having a higher SNR switches to higher bandwidth FSO link having a lower SNR if the received SNR of FSO link is above a switching threshold. So, the normalized capacity decreases upto a certain optical

$$\bar{C}_{\text{Total}} = \frac{2^{\alpha+\beta-2}}{\pi \ln(2)\Gamma(\alpha)\Gamma(\beta) B\left(\gamma_{\text{th}}^{\text{op}}+1\right)} \sum_{k=0}^{\infty} \frac{\left(-\gamma_{\text{th}}^{\text{op}} B\right)^k}{k!} G_{7,3}^{1,7}\left(\frac{1}{B\left(\gamma_{\text{th}}^{\text{op}}+1\right)} \middle| \begin{matrix} \chi_2 \\ \chi_3 \end{matrix} \right) + \frac{2^{\alpha+\beta-2} \ln\left(1+\gamma_{\text{th}}^{\text{op}}\right)}{\pi \ln(2)\Gamma(\alpha)\Gamma(\beta)} G_{1,5}^{5,0}\left(\gamma_{\text{th}}^{\text{op}} B \middle| \begin{matrix} 1 \\ \chi_1 \end{matrix} \right)$$
$$+ \frac{2^{\alpha+\beta+\delta_0-3}(\pi)^{-\frac{3}{2}}}{\ln(2)\Gamma(\delta_0)\Gamma(\alpha)\Gamma(\beta)} G_{1,5}^{4,1}\left(\frac{\alpha^2\beta^2 z}{16\bar{\gamma}_{\text{op}}} \middle| \begin{matrix} 1 \\ \chi_1 \end{matrix} \right) G_{3,5}^{5,1}\left(\frac{1}{4\Omega_0^2} \middle| \begin{matrix} 0, \frac{1}{2}, 1 \\ 0, \frac{\delta_0}{2}, \frac{\delta_0+1}{2}, 0, \frac{1}{2} \end{matrix} \right). \quad (19)$$

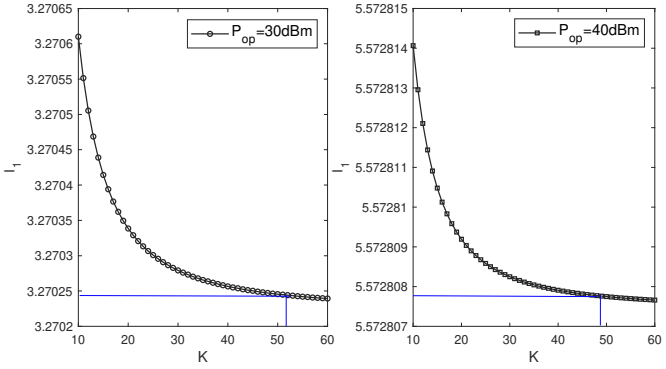

Fig. 2: The value of I_1 as a function of number of terms in I_1.

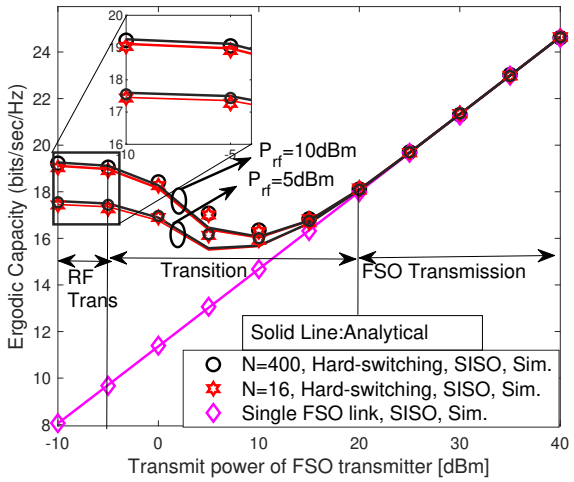

Fig. 3: Impact of P_{rf} and number of IRS elements on the ergodic capacity with $\gamma_{\text{th}}^{\text{op}}$=40 dB.

transmit power. During the transition period, the transmission link can be either RF link or FSO link depending on FSO link condition even if the FSO transmission power is fixed. With a further increase in the FSO transmit power, it becomes the dominant link, leading to an increase in capacity as the transmit power of the FSO link rises and the value is independent of the number of phase-shifter elements at IRS. For example, the ergodic capacity increases from 18.91 bits/sec/Hz to 19.11 bits/sec/Hz as IRS elements increases from 16 to 400 at $P_{\text{op}} = -5$ dBm. After a certain transmit power of FSO link, transmission link switches from higher SNR RF link to lower SNR FSO link, if the received SNR of FSO link is above a switching threshold. At this

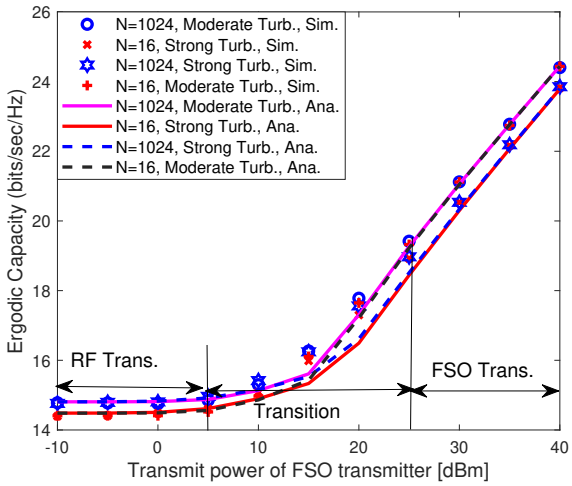

Fig. 4: The ergodic capacity for different numbers of phase shift elements at IRS under strong and moderate turbulence standards with $\gamma_{\text{th}}^{\text{op}}$ = 40 dB, and P_{rf} = 10 dBm.

transition period, transmission link can be either RF link or FSO link depending on FSO link condition even if the FSO transmission power is fixed.

Fig. 4 shows the ergodic capacity of hybrid RF/FSO system under moderate and strong turbulence for $N = 16, 1024$. The d_{sd}, d_{sr}, and d_{rd} are considered as 1200 m, 1160 m, and 60 m, respectively. The (α, β) vary with the severity of turbulence and their values are computed based on (2) and (3) and given in Table II. In this setup, the RF link is the main transmission link at lower P_{op}, and the atmospheric turbulence has minimal affect on RF channel. Thus the ergodic capacity at the lower regime of transmit power of the FSO link is unaffected by turbulence. In the transition region, the number of phase-shifter elements at IRS and atmospheric turbulence both affect the ergodic capacity. However, at higher values of P_{op}, the primary transmission link is the FSO link, which is significantly impacted by atmospheric turbulence and is unaffected by the IRS elements count. The ergodic capacity achieved under moderate turbulence and strong turbulence are different. The impact of number of phase-shifter elements at IRS is insignificant in this regime since active transmission link is the FSO one.

Fig. 5 presents the ergodic capacity for different link distances between the source-destination for two different numbers of reflected elements at the IRS, namely, $N = 16, 400$. The d_{sd}, d_{sr} and d_{rd} are considered as 500 m, 460 m, 60 m, and 1000 m, 960 m, 60 m, respectively. The link distances have significant effects on the large scale (α)

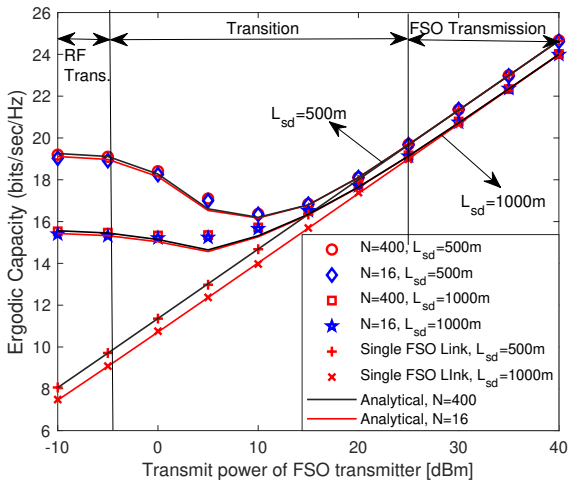

Fig. 5: The ergodic capacity for different source-destination link distances with $\gamma_{\rm th}^{\rm op}$ = 40 dB, and $P_{\rm rf}$ = 10 dBm.

and small scale (β) scintillation parameters, governed by (2) and (3). In this setup, the RF link is the main transmission link in the lower transmit power regime with the FSO link being active in the higher transmit power regime. Thus, the impact of a number of reflecting elements at IRS in the RF link is noticeable for the lower transmit power of the FSO link. However the performance becomes independent of N at higher transmit power. The effects of the number of phase-shifter elements gradually decrease as the FSO transmit power increases. However, the impact of distance is noticeable throughout the transmit power regime of FSO link as distance affects both RF and FSO transmissions.

V. Conclusion

In this paper, the ergodic capacity of a hybrid RF/FSO system with hard-switching scheme is investigated. The closed-form expression for the ergodic capacity is derived. Validation of the derived closed-form expression is performed using Monte-Carlo simulation. The influence of IRS element count on ergodic capacity has been presented, specifically at lower transmit power of the FSO link. The effects of moderate and strong turbulences and link distances on ergodic capacity have also been presented.

References

[1] S. Mondal, K. Singh, C.-P. Li, and S. Prakriya, "Mixed FSO/IRS-Aided NOMA Network with Heterogeneous Channels," in *Proc. WCNC*. IEEE, 2025, pp. 1–6.

[2] T. Rakia, H.-C. Yang, M.-S. Alouini, and F. Gebali, "Outage analysis of practical FSO/RF hybrid system with adaptive combining," *IEEE Commun. Lett.*, vol. 19, no. 8, pp. 1366–1369, Aug. 2015.

[3] I. S. Ansari, F. Yilmaz, and M.-S. Alouini, "Impact of pointing errors on the performance of mixed RF/FSO dual-hop transmission systems," *IEEE Wireless Commun. Lett.*, vol. 2, no. 3, pp. 351–354, Jun. 2013.

[4] H. Lei, H. Luo, K.-H. Park, Z. Ren, G. Pan, and M.-S. Alouini, "Secrecy outage analysis of mixed RF-FSO systems with channel imperfection," *IEEE Photon. J.*, vol. 10, no. 3, pp. 1–13, Jun. 2018.

[5] E. Illi, F. El Bouanani, and F. Ayoub, "A performance study of a hybrid 5G RF/FSO transmission system," in *Proc. Int. Conf. Wireless Netw. Mobile Commun. (WINCOM)*. IEEE, Nov. 2017, pp. 1–7.

[6] N. Vishwakarma and R. Swaminathan, "On the capacity performance of hybrid FSO/RF system with adaptive combining over generalized distributions," *IEEE Photon. J.*, vol. 14, no. 1, pp. 1–12, Feb 2022.

[7] M. Usman, H.-C. Yang, and M.-S. Alouini, "Practical switching-based hybrid FSO/RF transmission and its performance analysis," *IEEE Photon. J.*, vol. 6, no. 5, pp. 1–13, Oct. 2014.

[8] L. Huang, S. Liu, P. Dai, M. Li, G.-K. Chang, Y. Shi, and X. Chen, "Unified performance analysis of hybrid FSO/RF system with diversity combining," *J. Lightw. Technol.*, vol. 38, no. 24, pp. 6788–6800, Dec. 2020.

[9] E. S. Altubaishi and W. A. Alathwary, "On the capacity of decode-and-forward FSO system with single-and dual-hop RF link," *IEEE Photon. J.*, vol. 16, no. 1, pp. 1–8, 2023.

[10] P. K. Singya, B. Makki, A. D'Errico, and M.-S. Alouini, "Hybrid FSO/THz-based backhaul network for mmwave terrestrial communication," *IEEE Trans. Wireless Commun.*, vol. 22, no. 7, pp. 4342–4359, 2022.

[11] S. Mondal, K. Singh, C. Pan, and C.-P. Li, "Performance Analysis of STAR-IRS-aided MISO-ISAC Systems with Multiple Targets: A Rate-Splitting Approach," *IEEE Trans. Commun.*, Early access 2025.

[12] Q. Wu and R. Zhang, "Towards smart and reconfigurable environment: Intelligent reflecting surface aided wireless network," *IEEE Commun. Mag.*, vol. 58, no. 1, pp. 106–112, Jan. 2020.

[13] E. Björnson, Ö. Özdogan, and E. G. Larsson, "Intelligent reflecting surface versus decode-and-forward: How large surfaces are needed to beat relaying?" *IEEE Wireless Commun. Lett.*, vol. 9, no. 2, pp. 244–248, Feb. 2020.

[14] Z. Abdullah, G. Chen, S. Lambotharan, and J. A. Chambers, "A hybrid relay and intelligent reflecting surface network and its ergodic performance analysis," *IEEE Wireless Commun. Lett.*, vol. 9, no. 10, pp. 1653–1657, Oct. 2020.

[15] L. Yang, W. Guo, and I. S. Ansari, "Mixed dual-hop FSO-RF communication systems through reconfigurable intelligent surface," *IEEE Commun. Lett.*, vol. 24, no. 7, pp. 1558–1562, Jul. 2020.

[16] A. Sikri, A. Mathur, P. Saxena, M. R. Bhatnagar, and G. Kaddoum, "Reconfigurable intelligent surface for mixed FSO-RF systems with co-channel interference," *IEEE Commun. Lett.*, vol. 25, no. 5, pp. 1605–1609, May 2021.

[17] S. Mondal, K. Singh, C.-P. Li, and Z. Ding, "Hybrid FSO/Active IRS-aided NOMA-IoT Communications under Imperfect CSI and SIC," in *Proc. Globecom*. IEEE, 2024, pp. 2888–2893.

[18] ——, "Mixed FSO/active IRS-aided MISO NOMA communication with imperfect CSI and sic," *IEEE Internet Things J.*, vol. 12, no. 1, pp. 623–636, Jan. 2025.

[19] I. S. Gradshteyn and I. M. Ryzhik, *Table of integrals, series, and products*. Academic press, 2014.

[20] *Wolfram Research Inc., Mathematica Edition: Version 8, Champaign, IL, USA, 2010. [Online].* Available at https://functions.wolfram.com/HypergeometricFunctions/MeijerG/.

[21] T. Van Chien, L. T. Tu, S. Chatzinotas, and B. Ottersten, "Coverage probability and ergodic capacity of intelligent reflecting surface-enhanced communication systems," *IEEE Commun. Lett.*, vol. 25, no. 1, pp. 69–73, Jan. 2021.

[22] Y. Ai, A. Felipe, L. Kong, M. Cheffena, S. Chatzinotas, and B. Ottersten, "Secure vehicular communications through reconfigurable intelligent surfaces," *IEEE Trans. Veh. Technol.*, vol. 70, no. 7, pp. 7272–7276, Jul. 2021.

[23] A. P. Prudnikov, I. A. Brychkov, and O. I. Marichev, *Integrals and series: special functions*. CRC press, 1986, vol. 2.

[24] R. Singh, M. Rawat, and A. Jaiswal, "On the performance of mixed FSO/RF SWIPT systems with secrecy analysis," *IEEE Syst. J.*, vol. 16, no. 1, pp. 339–350, Mar. 2022.